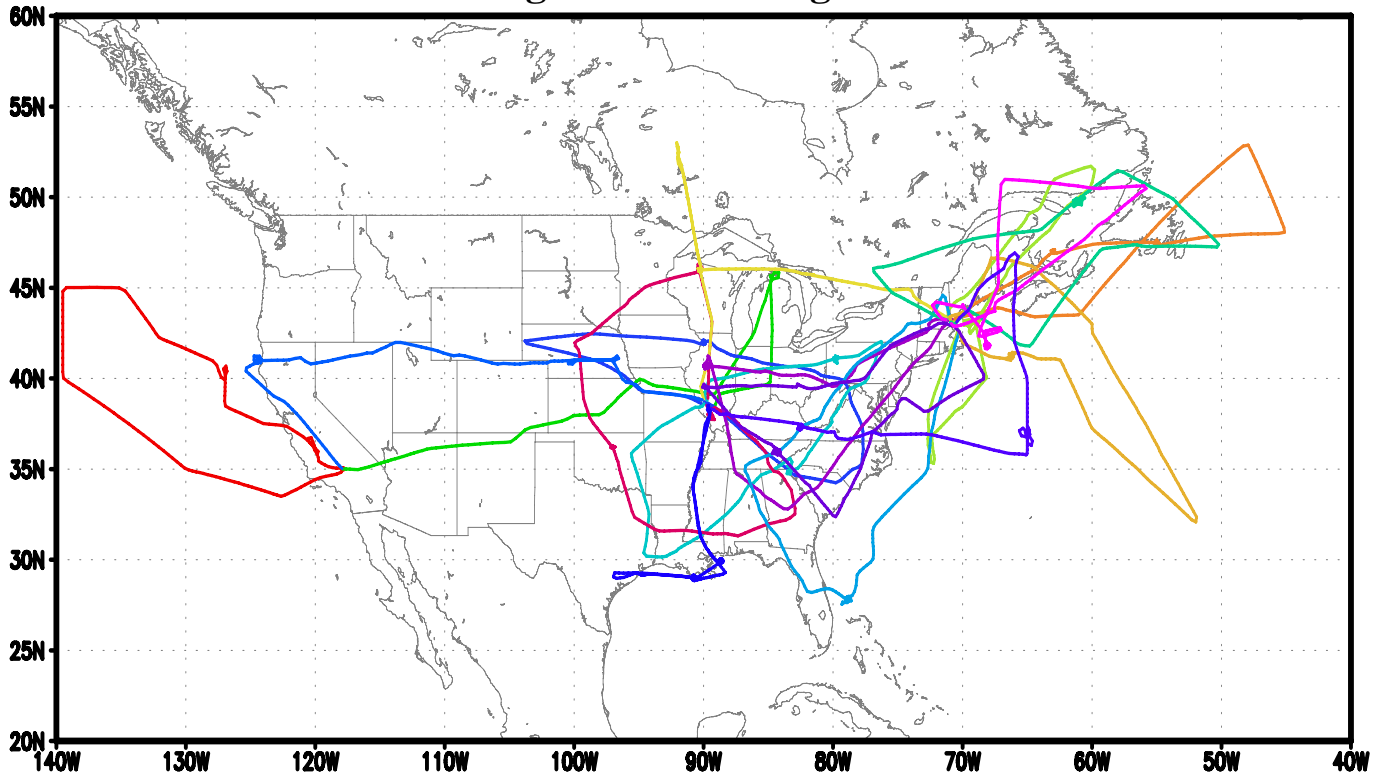


NASA DC-8 Flight Paths during ICARTT Period



NOAA WP-3 Flight Paths during ICARTT Period

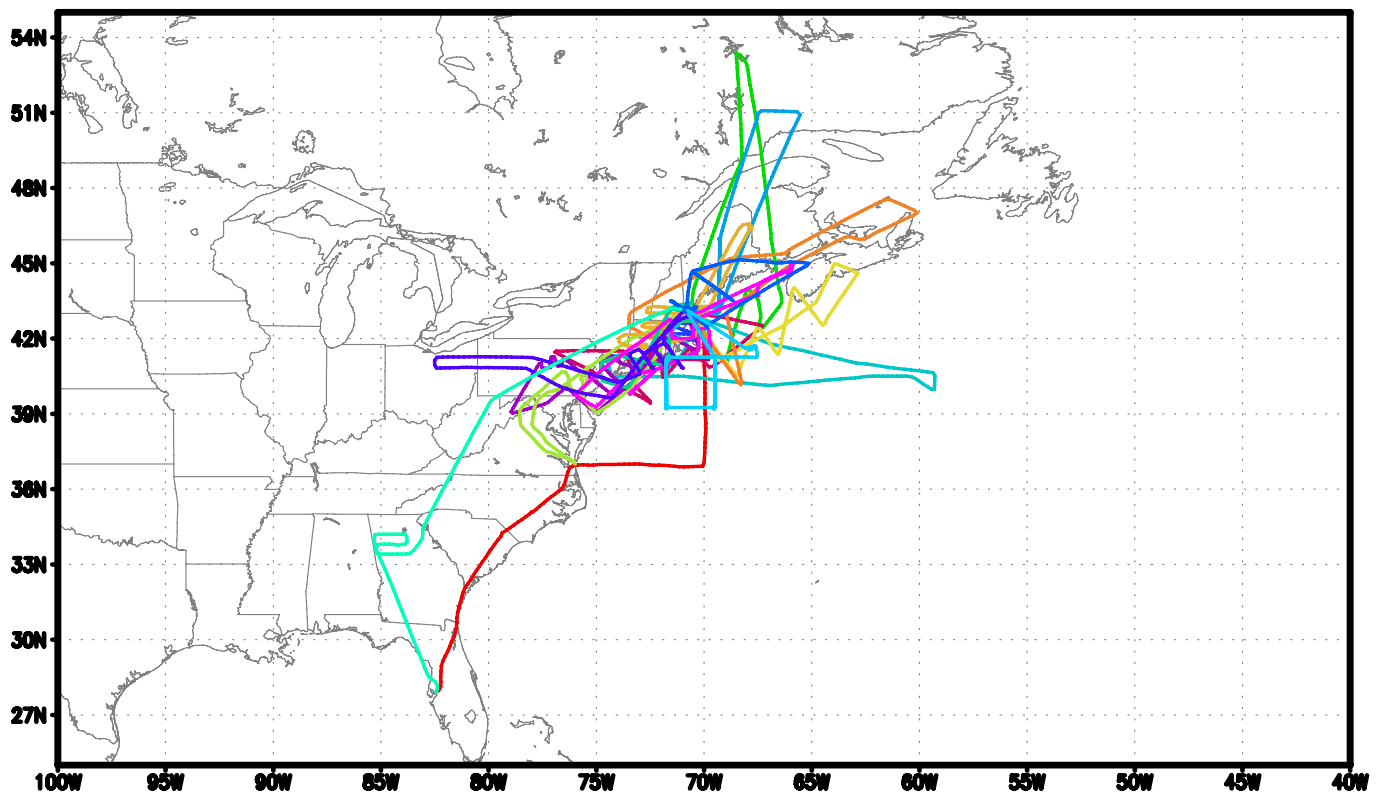


Figure 1. DC-8 and WP-3 flight paths during the ICARTT period. The colors show different flights.

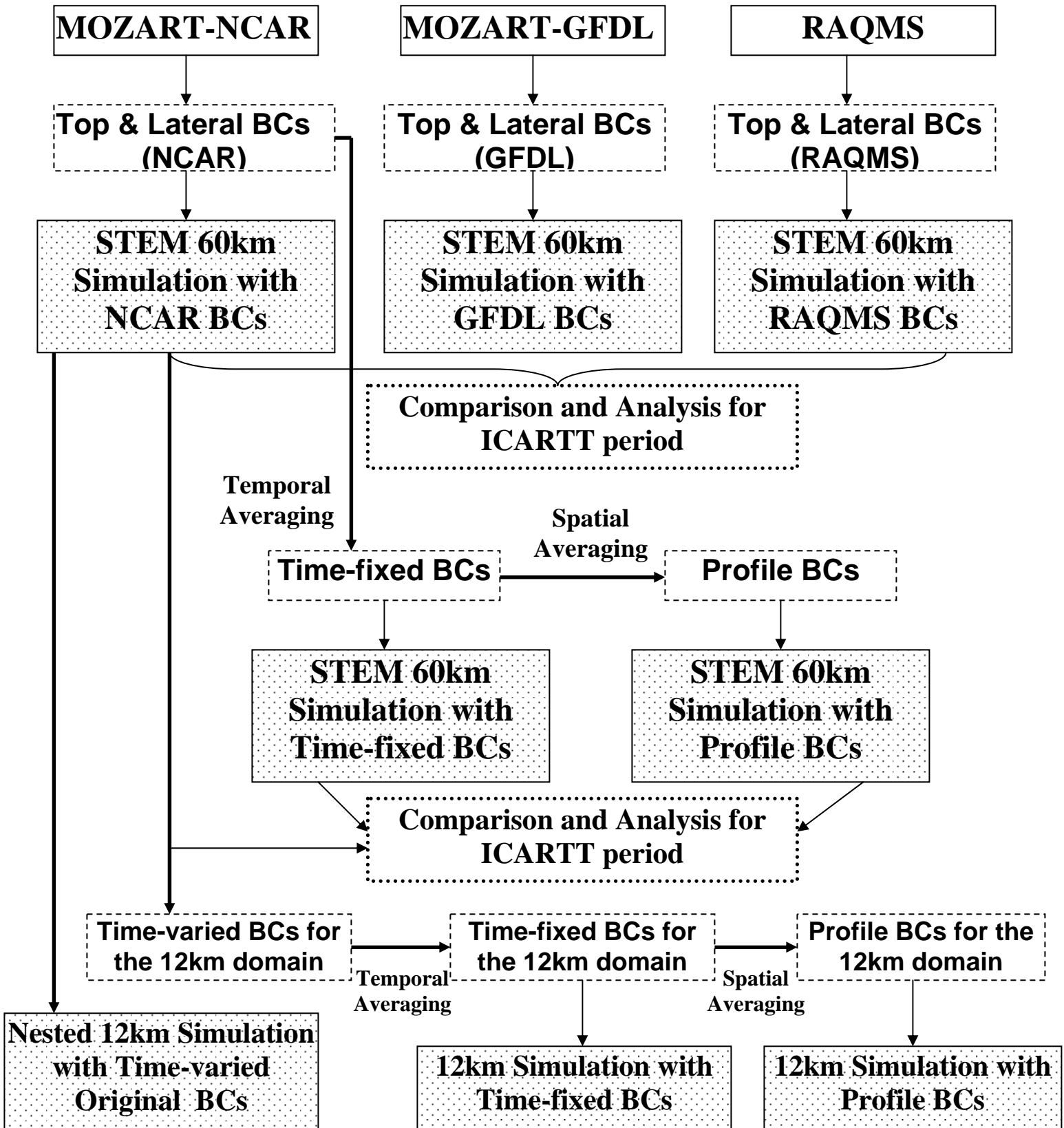
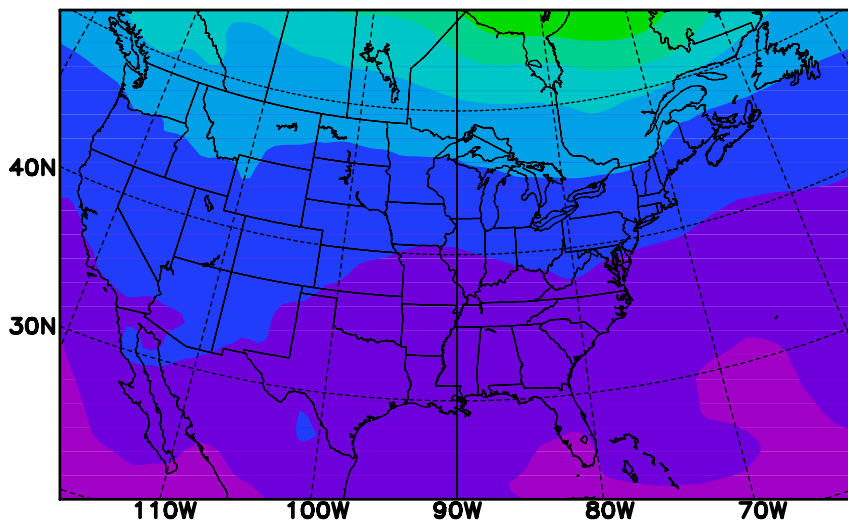
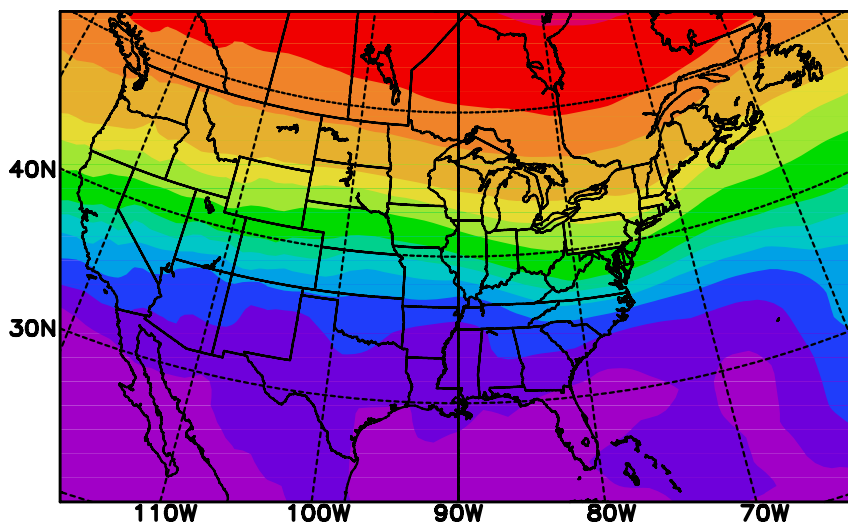


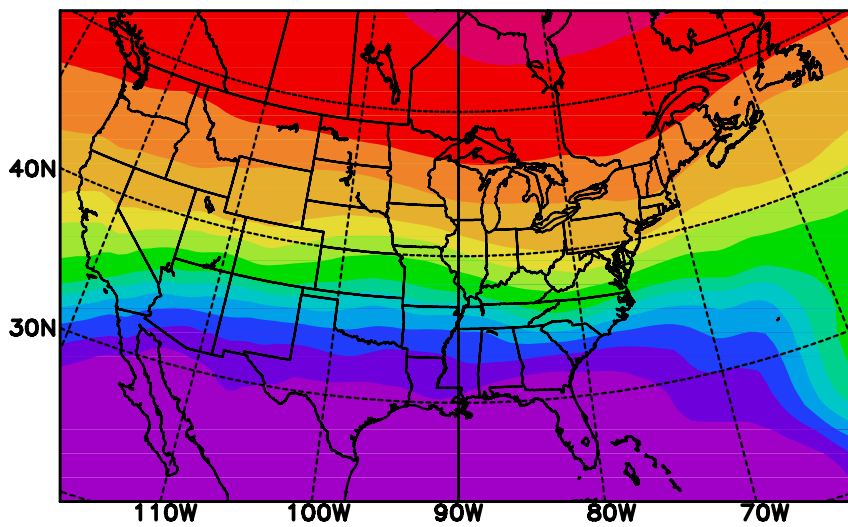
Figure 2. Comparison and Analysis Framework



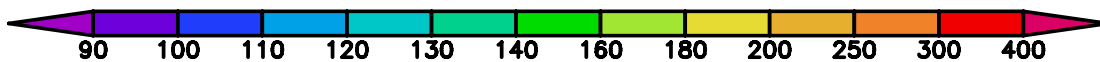
MOZART-NCAR



MOZART-GFDL



RAQMS



Mean O₃ top boundary conditions (ppbv) during the ICARTT period

Figure 3. Period-mean O₃ top boundary conditions from 3 global models.

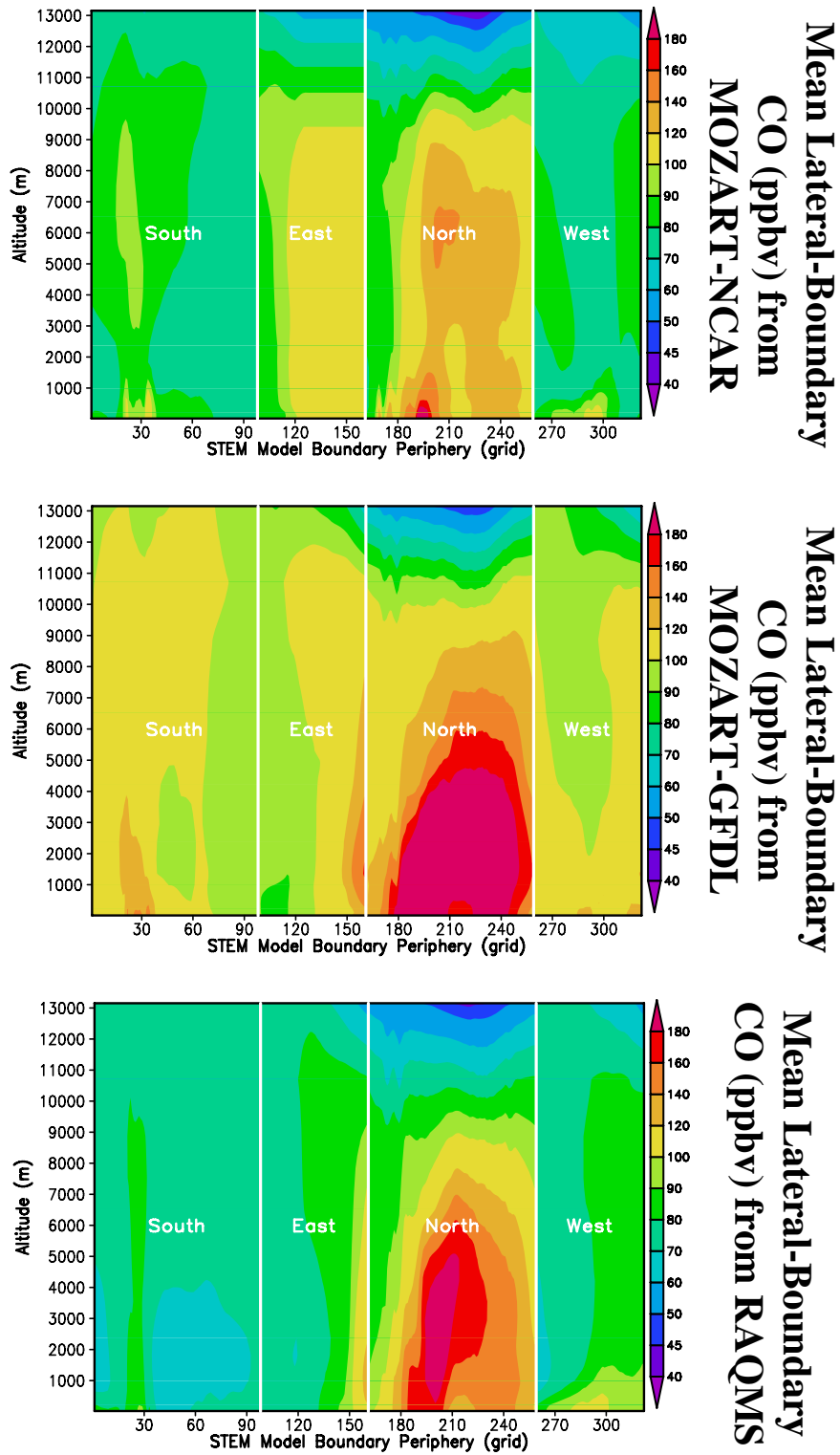


Figure 4. Period-mean CO lateral boundary conditions from 3 global models, along the STEM's boundary periphery in grid (60km) starting from the southwest corner of the STEM 60km domain shown in Figure 3.

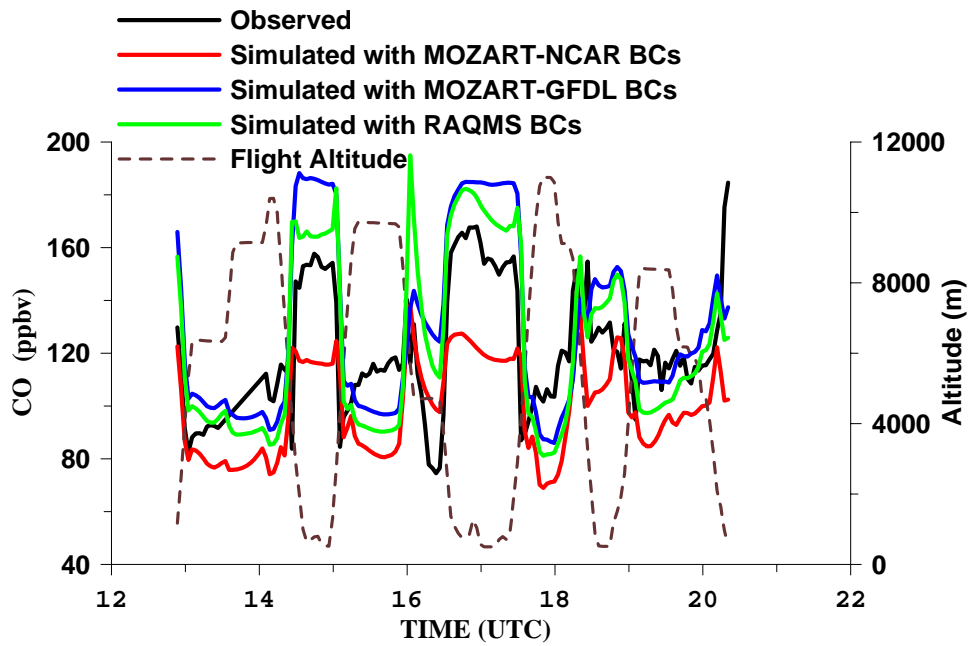
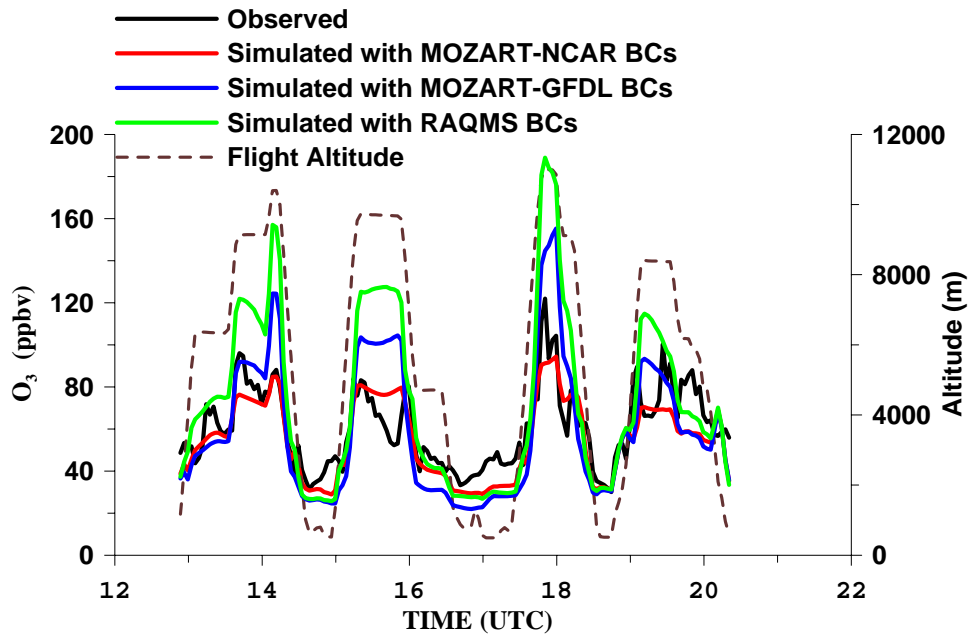


Figure 5. Observed and Simulated O₃ and CO concentrations for the DC-8 flight 8 on 07/15/2004

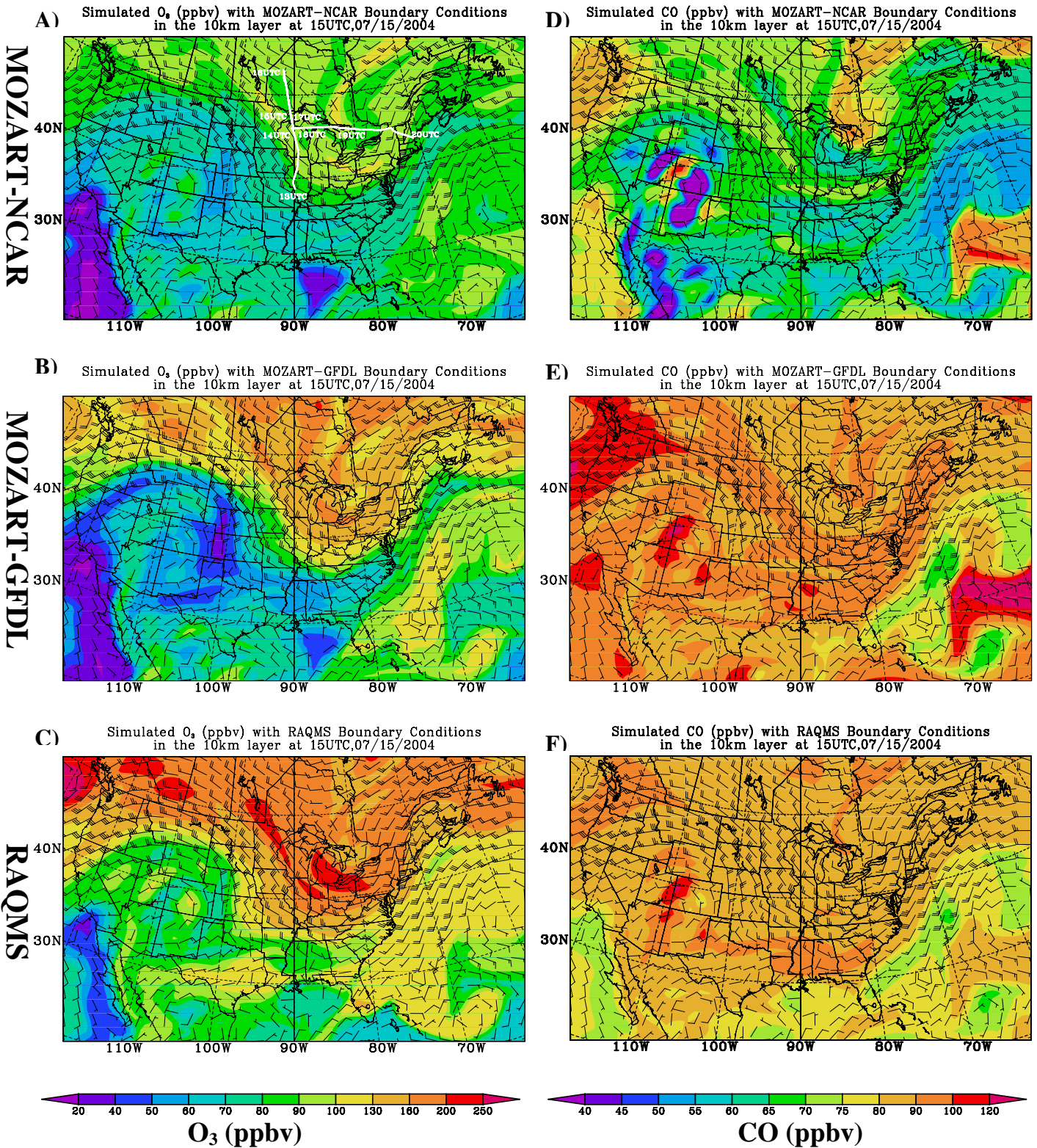


Figure 6. STEM 60km simulated O_3 and CO concentrations in the 10km layer with boundary conditions from the three global models for DC-8 flight 8 on July 15 (plot A shows the flight path).

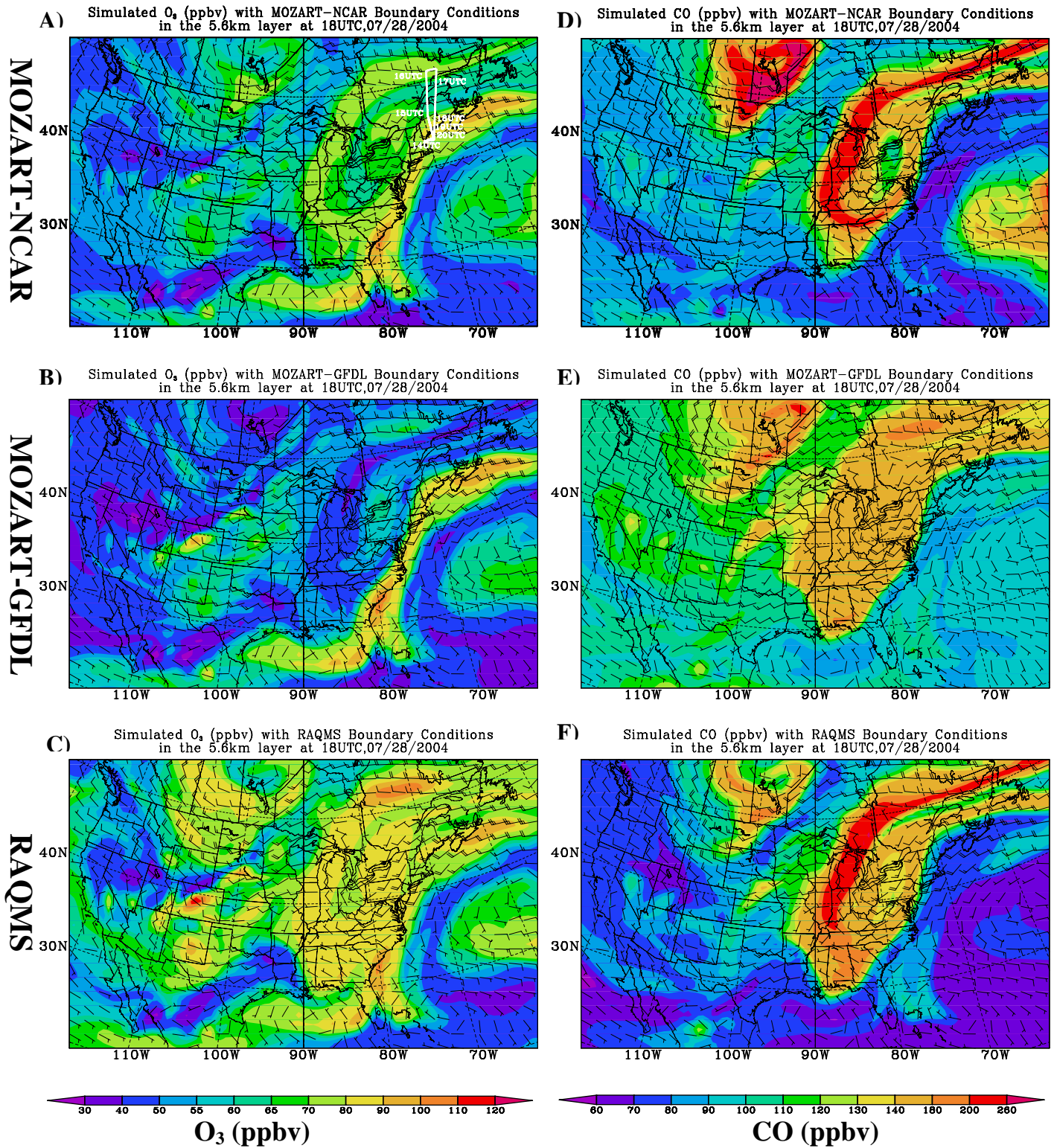


Figure 7. STEM 60km simulated O_3 and CO concentrations in the 5.6km layer with boundary conditions from the three global models for WP-3 flight 12 on July 28 (plot A shows the flight path).

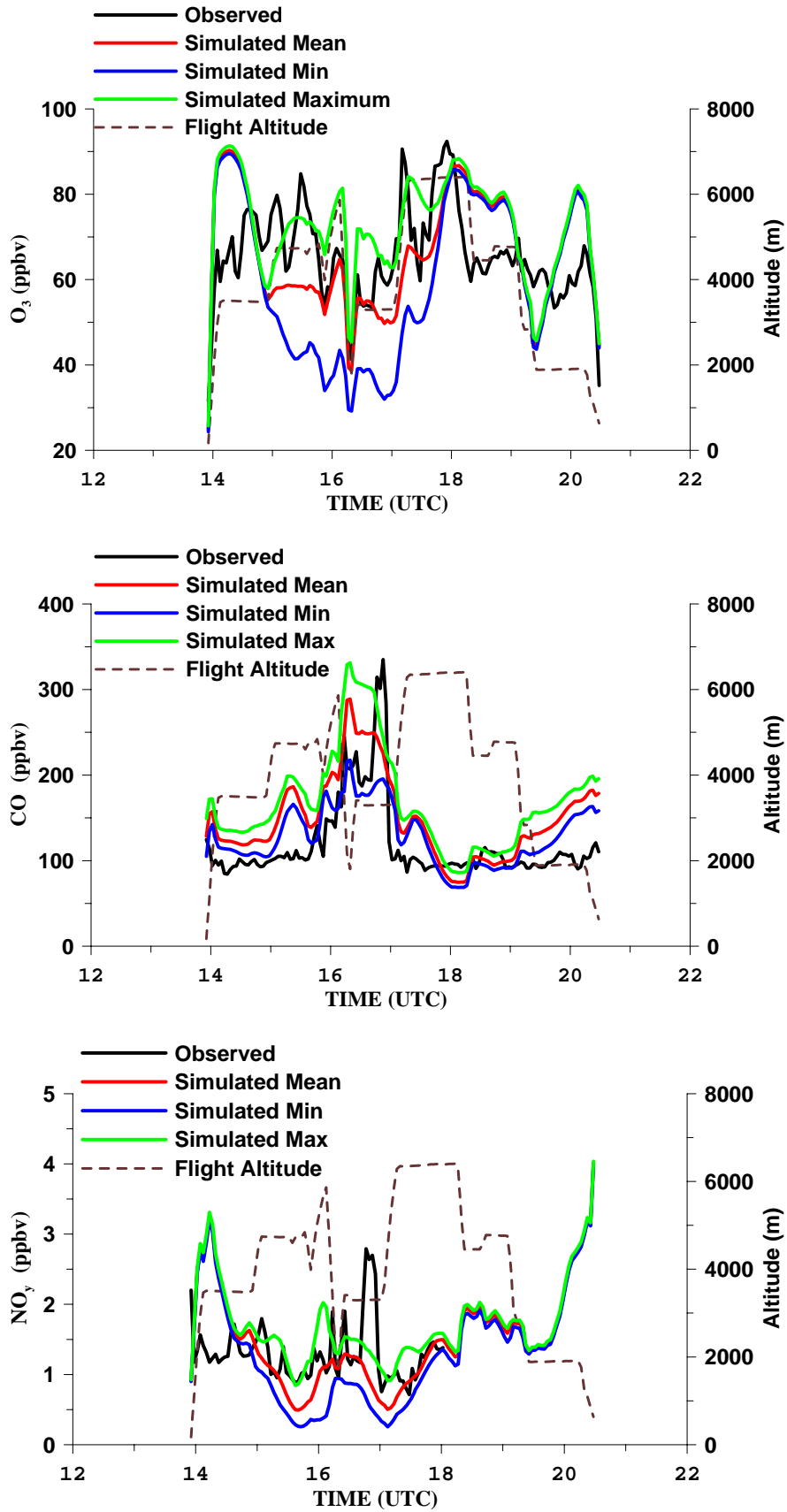


Figure 8. Observed and simulated mean/minimum/maximum O₃, CO, and NO_y concentrations for the WP-3 flight 12 on 07/28/2004

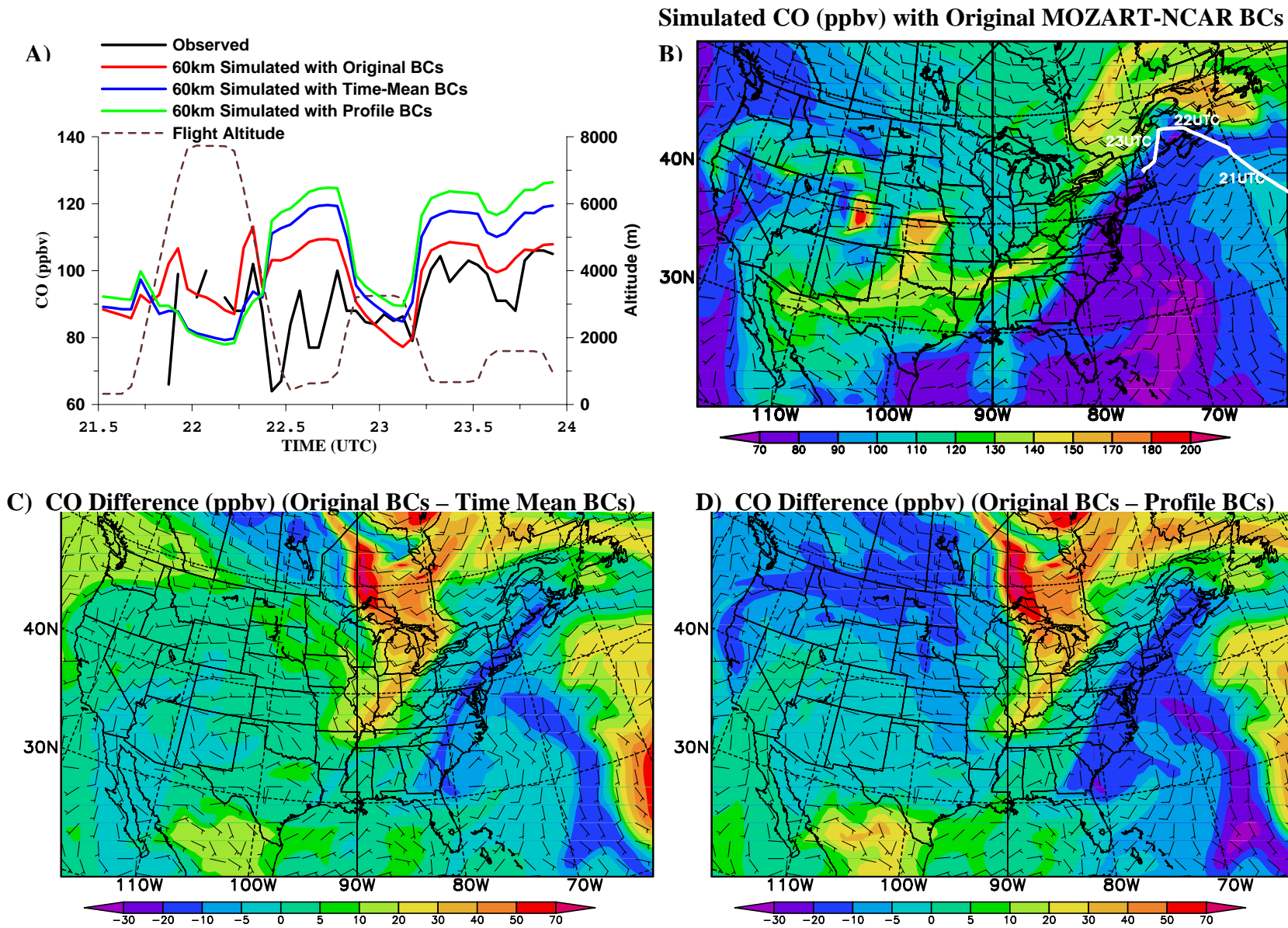


Figure 9. 60km simulated CO compared to the DC-8 flight observation on 07/31/2004. Plot B shows the simulated CO with original MOZART-NCAR BCs in the 3km layer, 0UTC, 08/01/2004. Plots C, D show the corresponding CO differences among the three simulations.

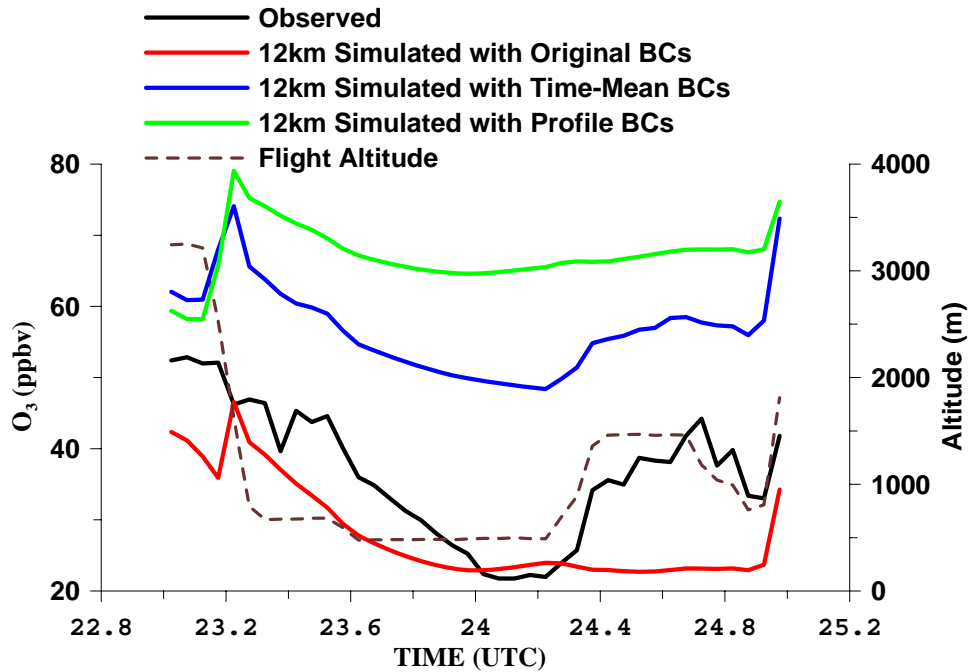
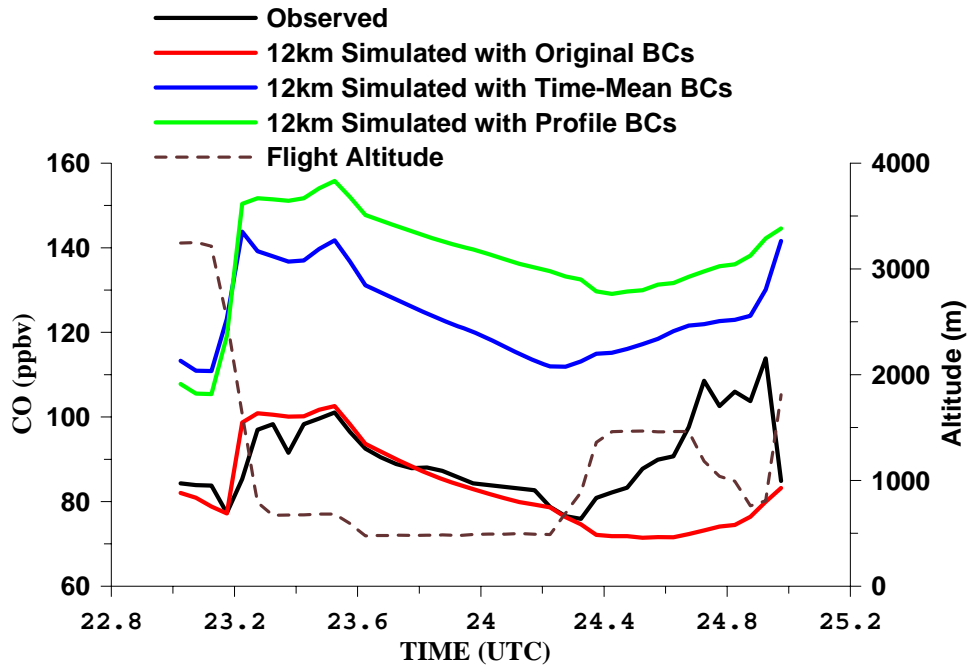


Figure 10. Observed and simulated CO and O₃ concentrations for the WP-3 flight 13 on 07/31- 08/01, 2004

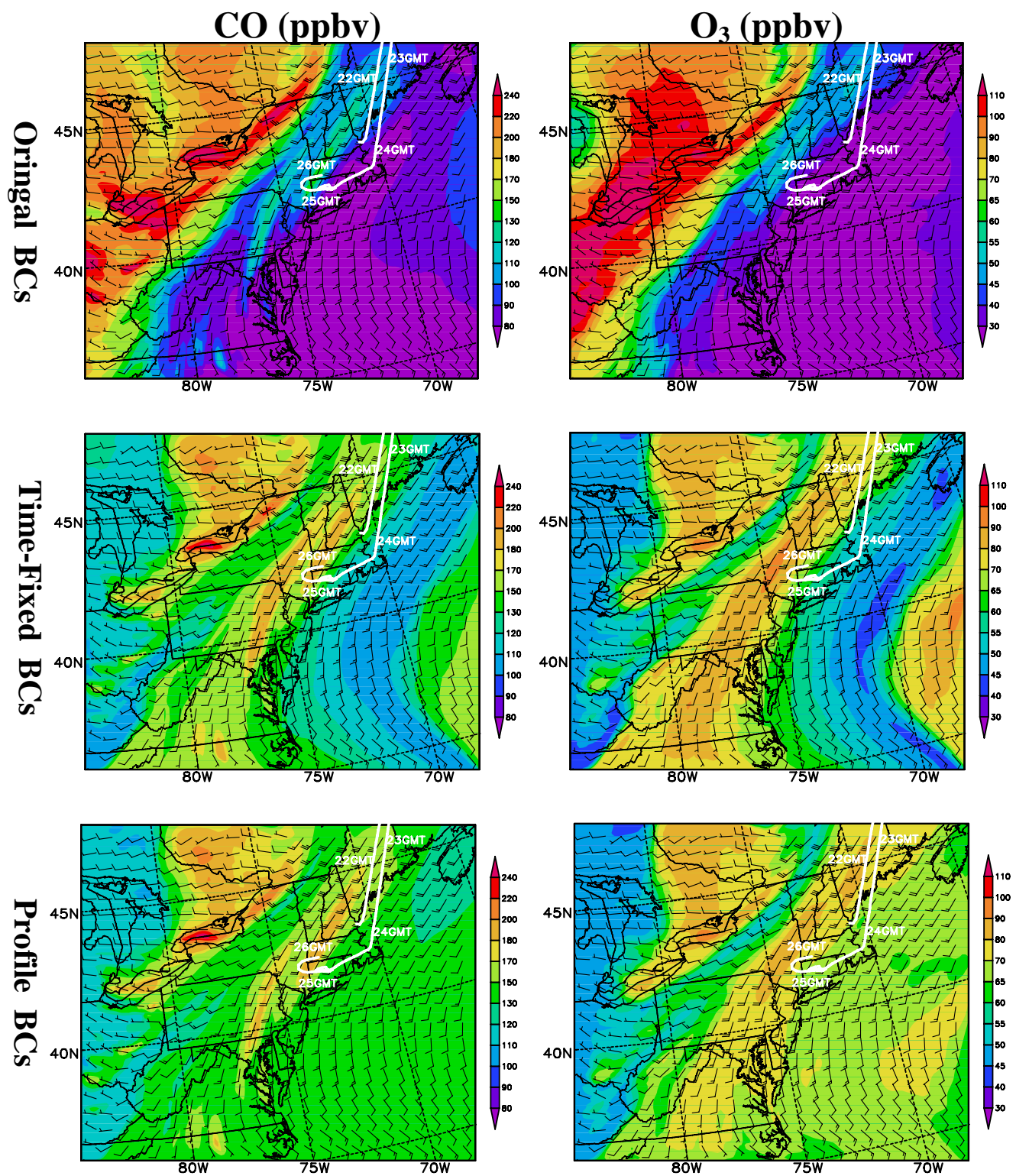


Figure 11. 12km simulated CO (left column) and O₃ (right column) concentrations in the 1km layer, at 0 UTC, 08/01/2004, driven by 3 different boundary conditions. The WP-3 flight path is shown in each plot.

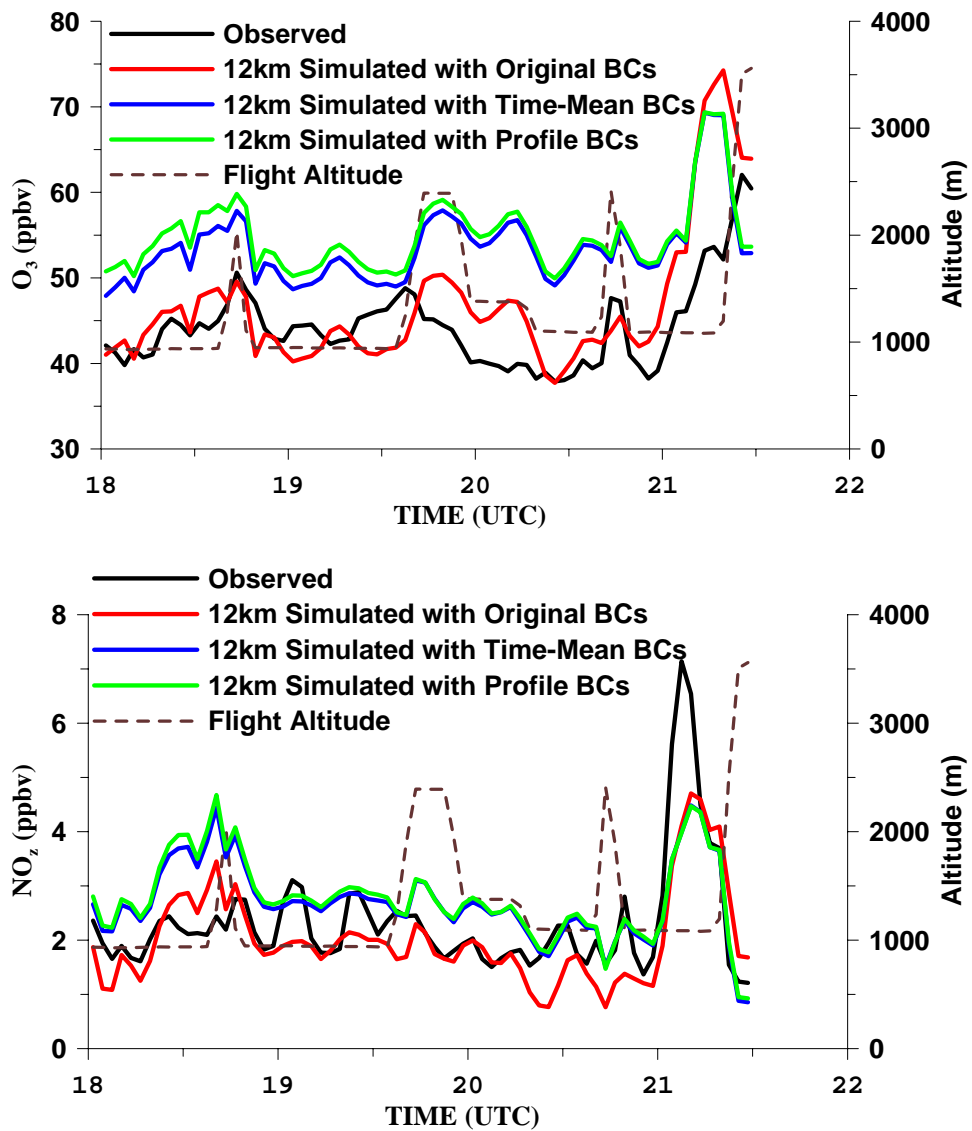
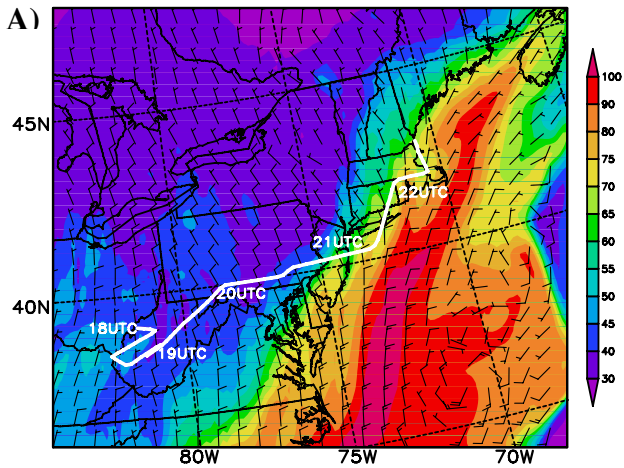
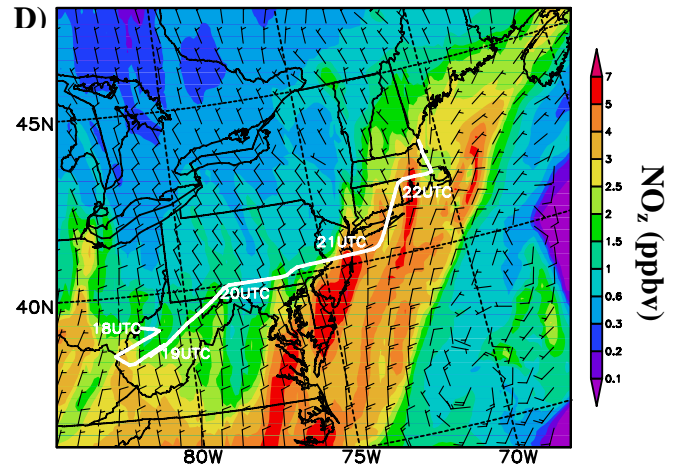


Figure 12. Observed and simulated O₃ and NO_z concentrations for the WP-3 flight 15 on 08/06/2004

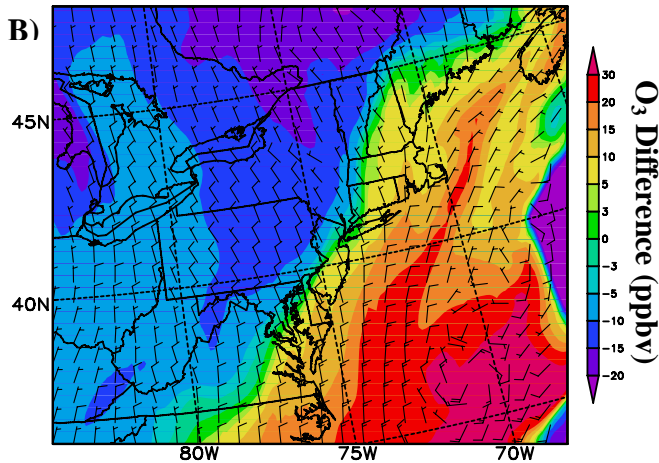
Simulated O₃ with original BCs



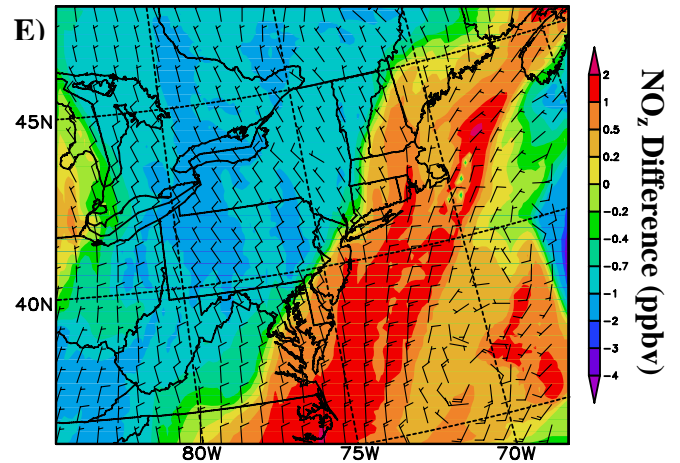
Simulated NO_z with original BCs



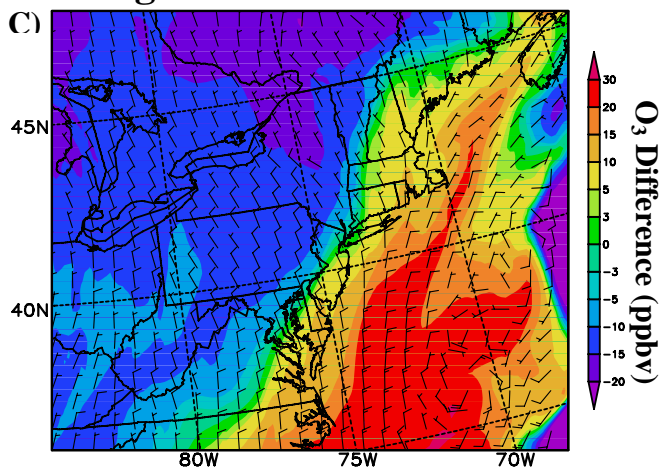
Original BCs – Time Fixed BCs



Original BCs – Time Fixed BCs



Original BCs – Profile BCs



Original BCs – Profile BCs

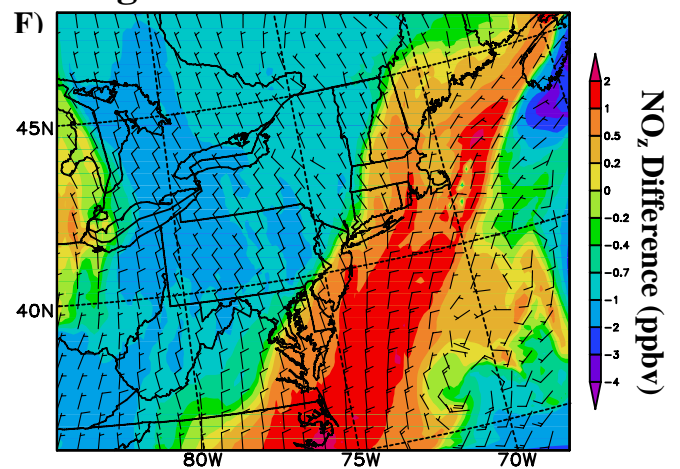


Figure 13. The 12km simulated O₃ and NO_z concentrations and their differences among the three simulations in the 1km layer, 18UTC, 08/06/2004.

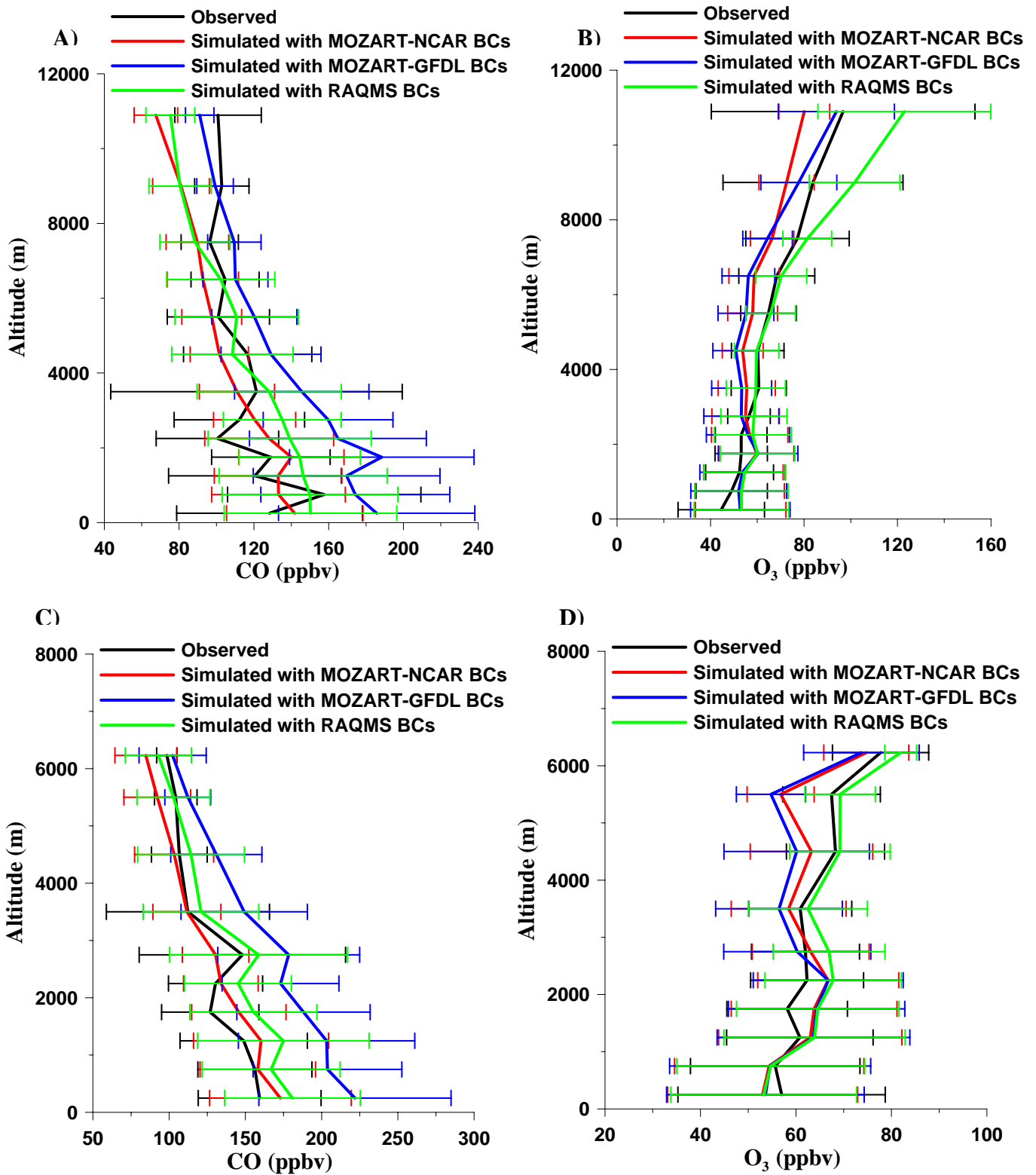


Figure 14. Observed and 60km-simulated CO and O₃ mean profiles and standard deviations for all DC-8 flights (A, B) and WP-3 flights (C, D)

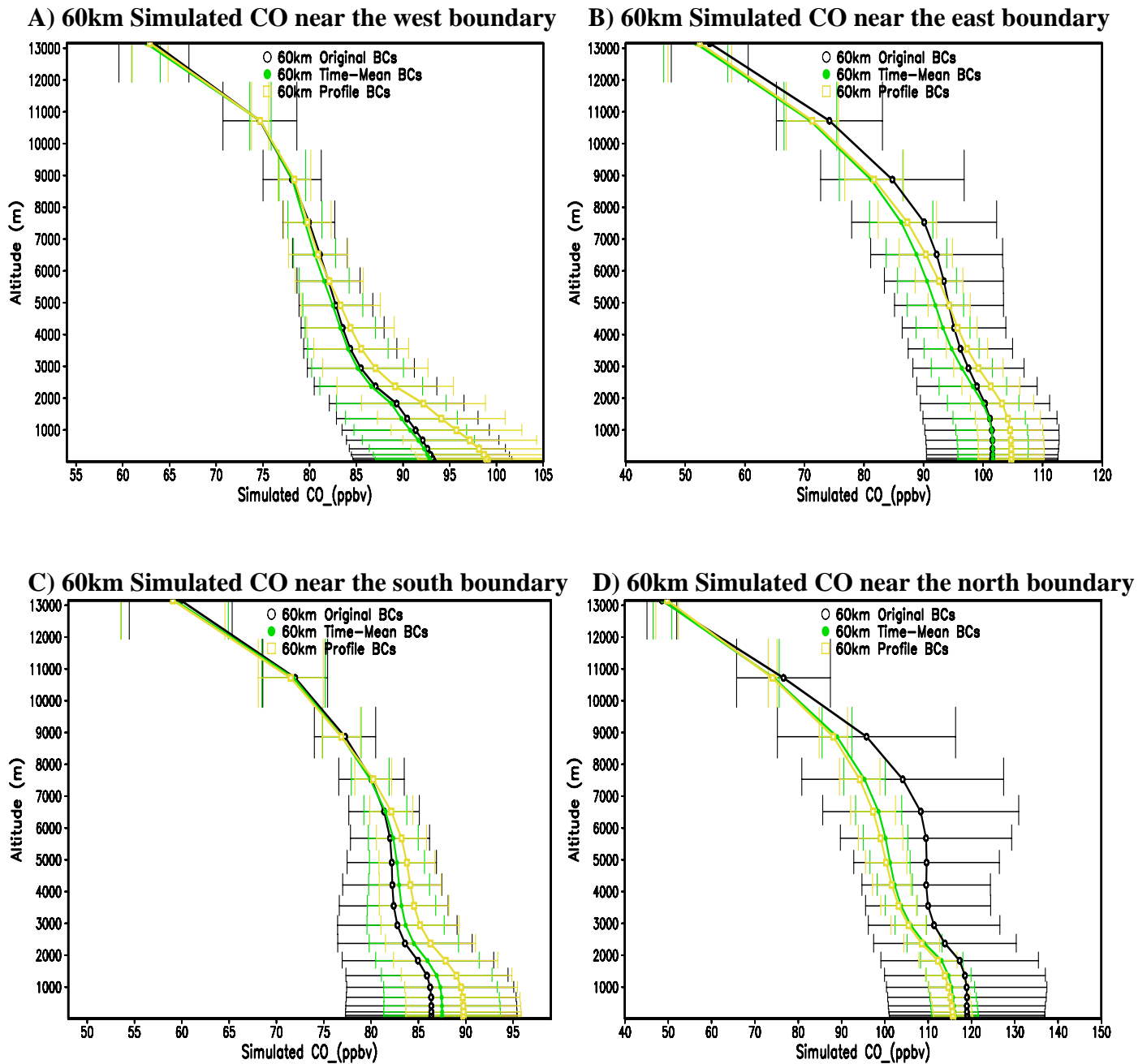


Figure 15. Simulated CO mean concentrations and standard deviation with original MOZART-NCAR, time-mean and profile boundary conditions over the grid lines that are 5 grid cells from west (A), east (B), south (C) and north (D) boundaries, respectively in the 60km domain.

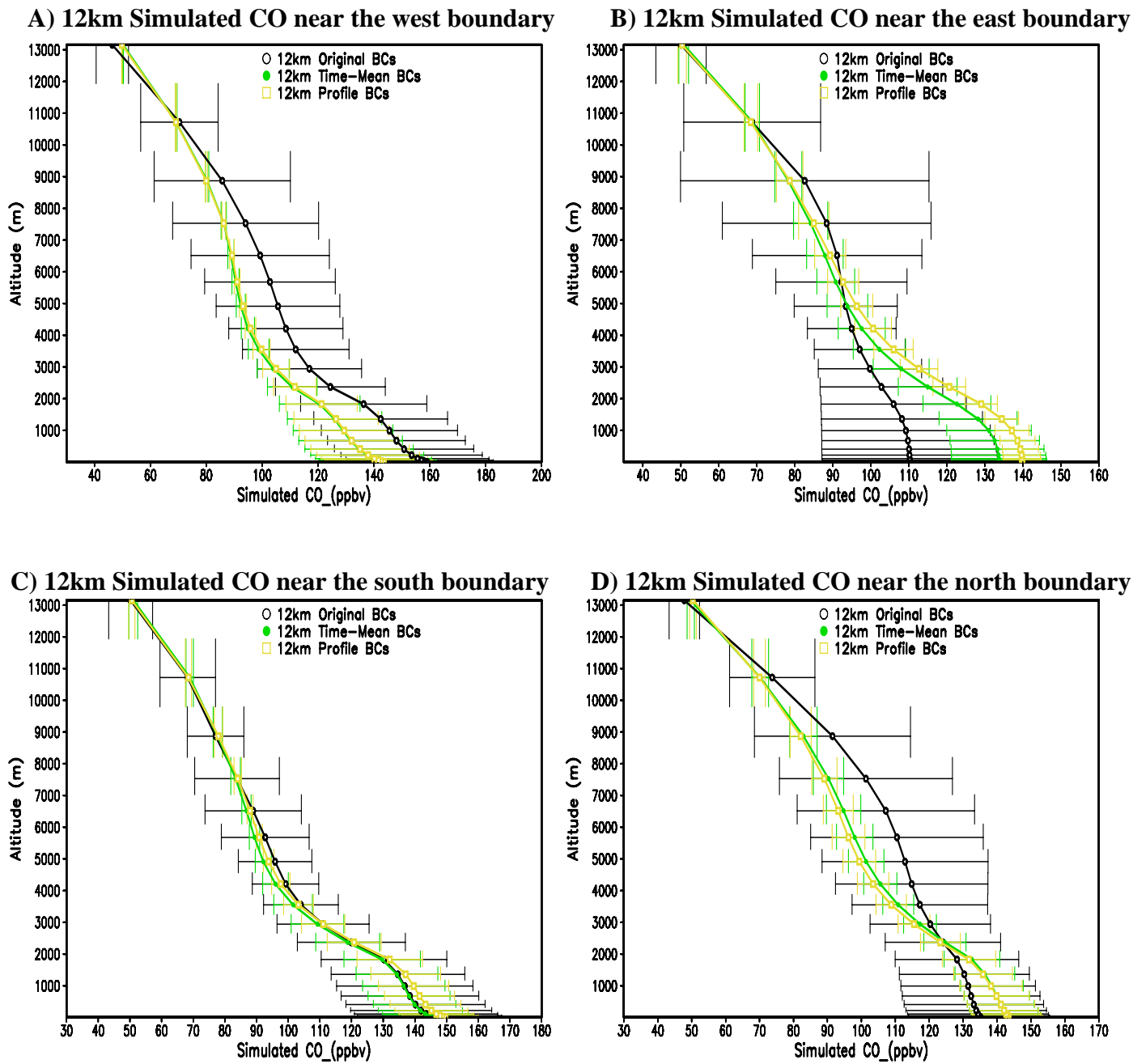


Figure 16. Simulated CO mean concentrations and standard deviation with original time-varied, time-mean and profile boundary conditions over the grid lines that are 5 grid cells from west (A), east (B), south (C) and north (D) boundaries, respectively in the 12km domain.

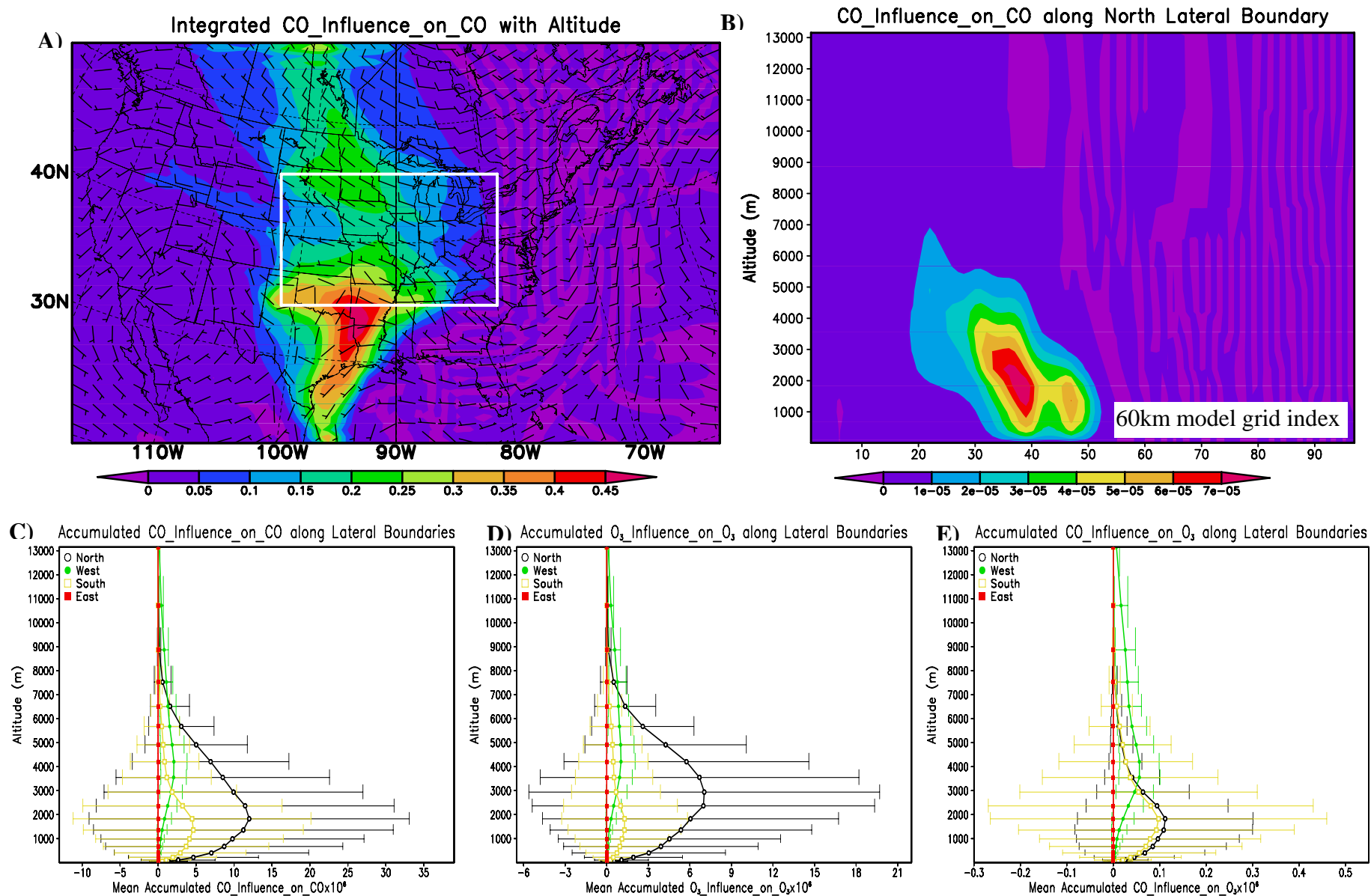


Figure 17. The influence function distributions: A) integrated with altitude and time-mean wind in 3km B) north boundary and C), D), E) mean and standard deviations along the 4 lateral boundaries. The influence functions are integrated from July 19 to 24 for the target grid box with vertical elevation 1-4km shown in panel A.